Electronic Supplementary Material (ESI) for Environmental Science: Processes & Impacts.

Supporting Information for:

Effects of Vertical Hydrodynamic Mixing on Photomineralization of Dissolved Organic Carbon in Arctic Surface Waters

Angang Li[1], Antoine F. Aubeneau[*2], Tyler King[3], Rose M. Cory[4], Bethany T. Neilson[3], Diogo Bolster[5], and Aaron I. Packman[1]

[1] Civil and Environmental Engineering, Northwestern University, Evanston, IL, USA
[2] Lyles School of Civil Engineering, Purdue University, West Lafayette, IN, USA
[3] Civil and Environmental Engineering, Utah State University, Logan, UT, USA
[4] Earth and Environmental Sciences, University of Michigan Ann Arbor, Ann Arbor, MI, USA
[5] Civil & Environmental Engineering and Earth Sciences, University of Notre Dame, Notre Dame, IN, USA

20 pages; 4 tables; 5 figures

Contents

Figure S1. Site map of the Kuparuk River on the North Slope of Alaska. Photochemical parameters were measured from water samples collected from the sampling sites[1] (red circles). River discharge and channel geometry data were collected from 8 gauging stations along the Kuparuk River[2] (blue crosses).

Figure S2. Summary of (A) photochemical parameters[3-6] (years 2011-2013) as a function of light wavelength and (B) hydrology parameters[2] (years 2013-2015) as a function of downstream distance in the Kuparuk River. Panel (A) contains spectra of photon flux at the water surface (Q_λ) from 19-June-2013, a sunny (clear sky) day at Toolik Field Station in Arctic Alaska, with different colors denoting different hours within a day, ±95% confidence interval of the light attenuation coefficient of CDOM ($aCDOM_\lambda$) and the photo-lability of CDOM (Φ_λ), and parameters α_λ and ε_λ that relate DOC concentration to $aCDOM_\lambda$. Panel (B) contains water surface slope (S), and ranges of water column depth (H), river width (W), and flow discharge (Q).

Figure S3. Spectra of light attenuation coefficient of CDOM ($aCDOM_\lambda$) and photo-lability of CDOM (Φ_λ) for arctic streams, rivers, and lakes[1, 7]. Parameters $aCDOM_\lambda$ and Φ_λ exhibit an exponential relationship with wavelength, with exponential slopes of -0.005 and -0.009, respectively. These slopes are based on log10 of $aCDOM_\lambda$ and Φ_λ, which is the same as exponential slopes -0.012 and -0.021 for natural log of $aCDOM_\lambda$ and Φ_λ.

Figure S4. Water column depth (H) and water surface slope (S) as a function of flow discharge (Q) for arctic stream, rivers, and beaded streams. Data sources are summarized in Table S1. Dash-dot lines represent 95% prediction intervals of the power law relationships of H-Q and S-Q.

Figure S5. Reaction efficiency heatmap of (A) beaded streams under slow flow, (B) shallow lakes, and (C) deep lakes. Natural variations of surface Damkohler number ($d*$) and dimensionless light attenuation ($p*$) values for each type of systems are plotted in white lines.

SI-1. No mixing limitation when CDOM is the only light attenuating constituent.
SI-2. Compiling photochemical and hydrological data of arctic waters.
SI-3. Non-dimensionalization of the dispersion-reaction equation.
SI-4. Solving for the depth-integrated photomineralization rate.
SI-5. Estimating vertical dispersion profiles of arctic waters.

Table S1. Data sources of photochemical and hydrological parameters in arctic stream, rivers, beaded streams, and lakes.
Table S2. Reported ranges (min, max) of photochemical and hydrological parameters in arctic streams and rivers (rocky bottom), beaded streams (peat bottom), and lakes.
Table S3. (A) Percentage of systems partially or substantially limited by mixing for each type of arctic systems that exhibit exponential light attenuation over depth. (B) Depth-integrated attenuation ratio (mean ± standard error) for each type of arctic systems that are partially or substantially limited by mixing.
Table S4. List of notations.

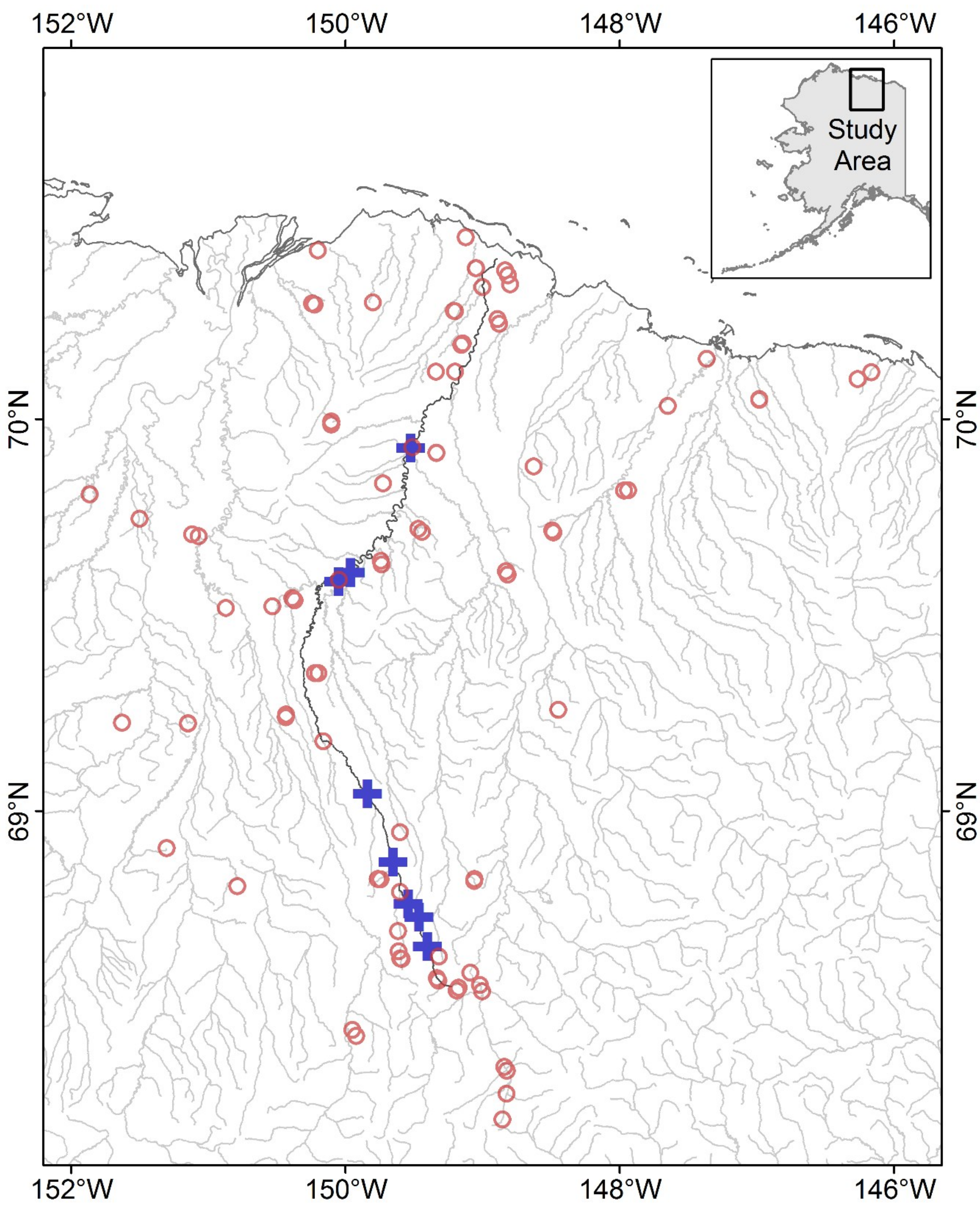

Figure S1. Site map of the Kuparuk River on the North Slope of Alaska. Photochemical parameters were measured from water samples collected from the sampling sites[1] (red circles). River discharge and channel geometry data were collected from 8 gauging stations along the Kuparuk River[2] (blue crosses).

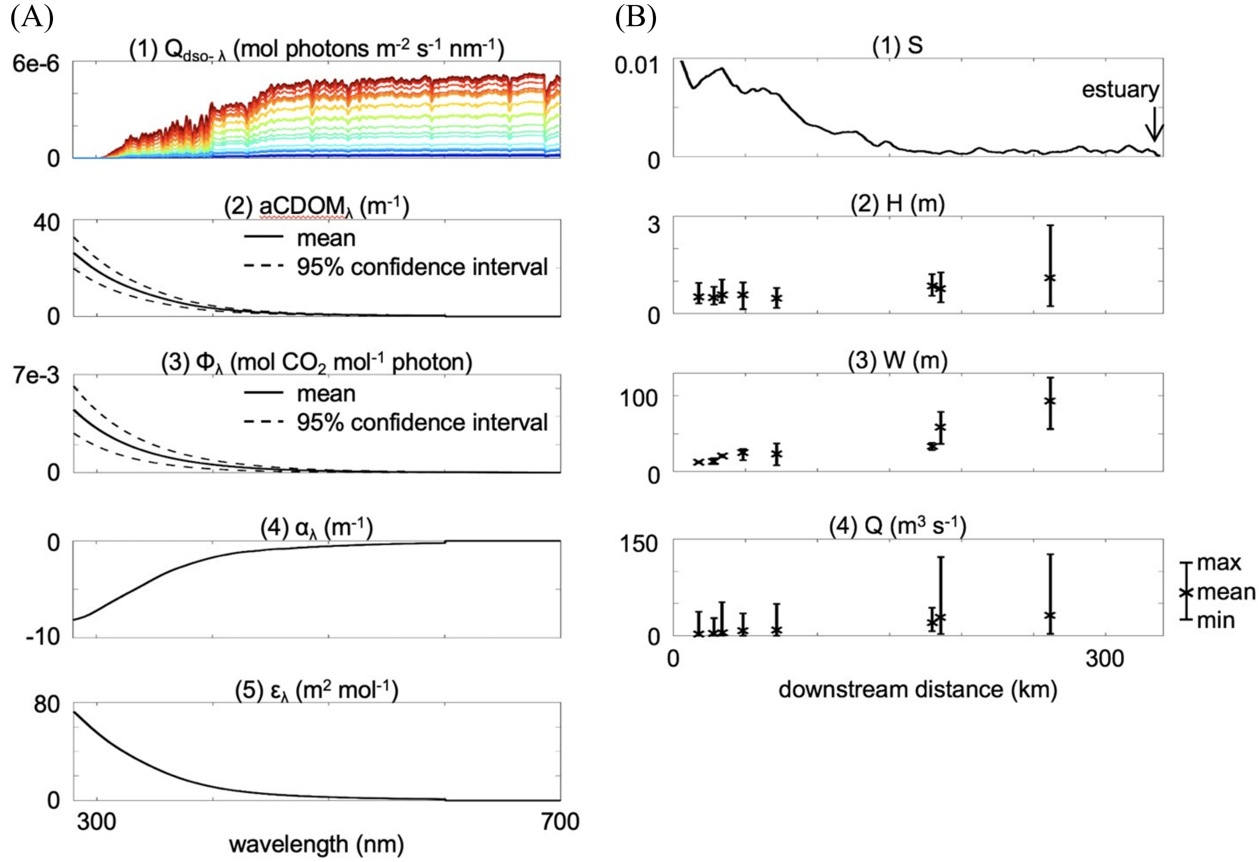

Figure S2. Summary of (A) photochemical parameters[3-6] (years 2011-2013) as a function of light wavelength and (B) hydrology parameters[2] (years 2013-2015) as a function of downstream distance in the Kuparuk River. Panel (A) contains spectra of photon flux at the water surface (Q_λ) from 19-June-2013, a sunny (clear sky) day at Toolik Field Station in Arctic Alaska, with different colors denoting different hours within a day, ±95% confidence interval of the light attenuation coefficient of CDOM ($aCDOM_\lambda$) and the photo-lability of CDOM (Φ_λ), and parameters α_λ and ε_λ that relate DOC concentration to $aCDOM_\lambda$. Panel (B) contains water surface slope (S), and ranges of water column depth (H), river width (W), and flow discharge (Q).

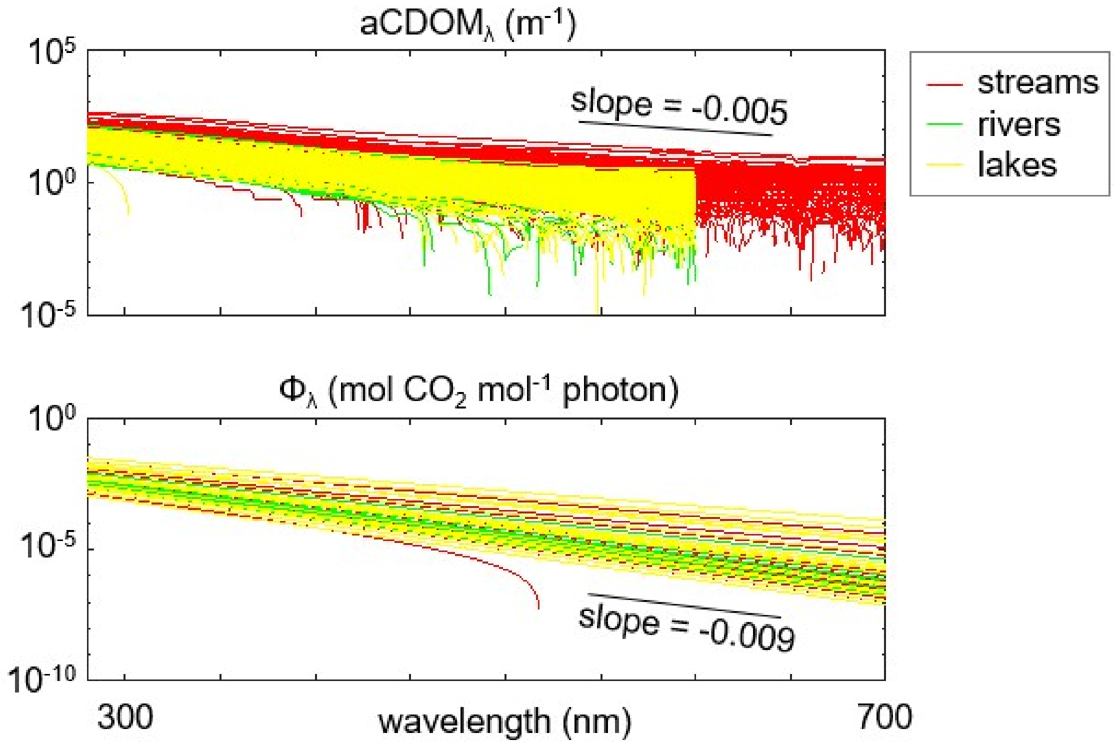

Figure S3. Spectra of light attenuation coefficient of CDOM ($aCDOM_\lambda$) and photo-lability of CDOM (Φ_λ) for arctic streams, rivers, and lakes[1,7]. Parameters $aCDOM_\lambda$ and Φ_λ exhibit an exponential relationship with wavelength, with decadic slopes of -0.005 and -0.009, respectively. These slopes are based on log10 of $aCDOM_\lambda$ and Φ_λ, which is the same as exponential slopes -0.012 and -0.021 for natural log of $aCDOM_\lambda$ and Φ_λ.

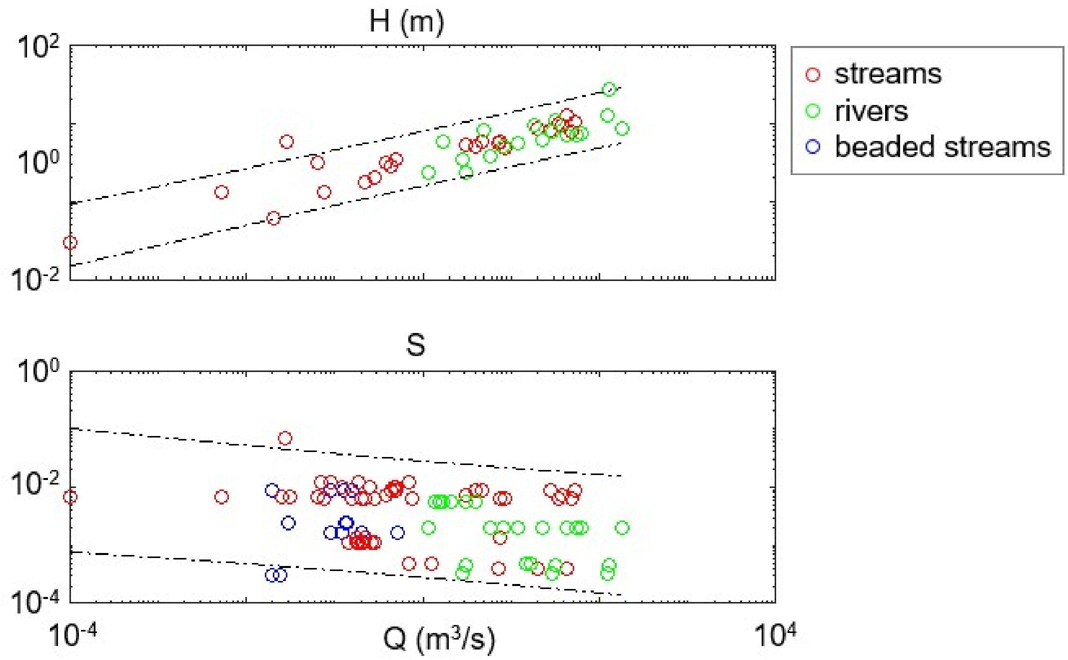

Figure S4. Water column depth (*H*) and water surface slope (*S*) as a function of flow discharge (*Q*) for arctic stream, rivers, and beaded streams. Data sources are summarized in Table S1. Dash-dot lines represent 95% prediction intervals of the power law relationships of *H*-*Q* and *S*-*Q*.

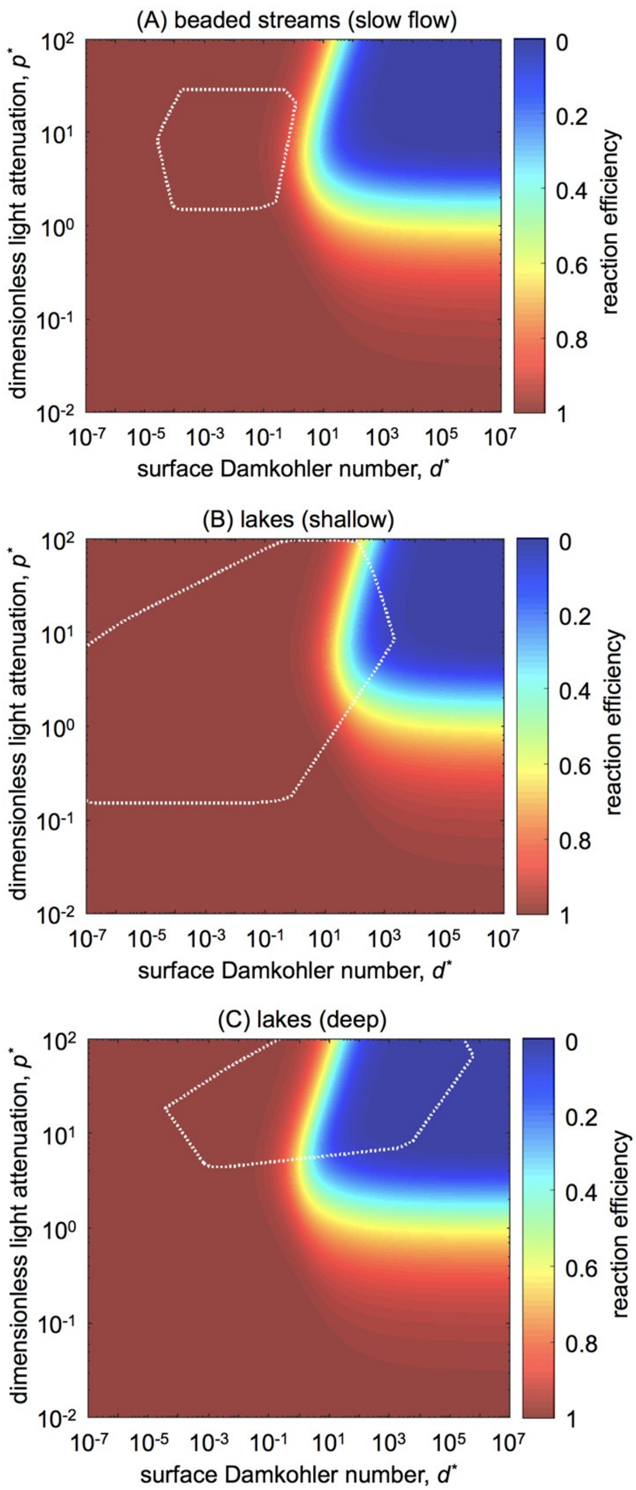

Figure S5. Reaction efficiency heatmap of (A) beaded streams under slow flow, (B) shallow lakes, and (C) deep lakes. Natural variations of surface Damkohler number (d^*) and dimensionless light attenuation (p^*) values for each type of systems are plotted in white lines.

SI-1. No mixing limitation when CDOM is the only light attenuating constituent.

When CDOM is the only light attenuating constituent, light does not necessarily decay exponentially with depth, especially when CDOM is nonhomogeneously distributed. At each vertical position (y) in the water column, photon flux ($Q_\lambda(y)$) depends on the total amount of CDOM above that position[8].

$$Q_\lambda(y) = Q_{dso-\lambda} e^{-\int_0^y aCDOM_\lambda(y)dy} \tag{S1}$$

where $Q_{dso\text{-}\lambda}$ is the photon flux at the water surface, $aCDOM_\lambda(y)$ is the light attenuation coefficient of CDOM, and λ is wavelength. The photomineralization rate profile ($PM(y)$) is the product of the photo-lability of CDOM to photomineralization (Φ_λ), the light attenuation coefficient of CDOM, and the photon flux[1].

$$PM(y) = \sum_\lambda \phi_\lambda aCDOM_\lambda(y) Q_{dso-\lambda} e^{-\int_0^y aCDOM_\lambda(y)dy} \tag{S2}$$

Using integration by parts and calculus theorem, the total attenuation of light across the water column (ΔQ_λ) can be derived as

$$\Delta Q_\lambda = Q_{dso-\lambda} - Q_{dso-\lambda} e^{-\int_0^H aCDOM_\lambda(y)dy} \tag{S3}$$

where the exponential term on the right-hand side of (S3) is a function of the total CDOM amount in the water column, so the total attenuation of light across the water column is the same regardless of the distribution of CDOM. Similarly, the upscaled photomineralization rate over the water column can be derived as

$$\int_0^H PM(y)dy = \phi_\lambda Q_{dso-\lambda}\left(1 - e^{-\int_0^H aCDOM_\lambda(y)dy}\right) \tag{S4}$$

which is independent of the distribution of CDOM. Therefore, in arctic waters where CDOM is the only constituent that attenuates light, upscaled phtomineralization rate over the water column is not limited by vertical hydrodynamic mixing.

SI-2. Compiling photochemical and hydrological data of arctic waters.

Spectra of light attenuation coefficient of CDOM ($aCDOM_\lambda$) and photo-lability of CDOM (Φ_λ) are available from over 1000 samples for arctic streams and rivers and over 2000 samples for arctic lakes[1, 7]. These spectra show exponential relationships with wavelength (Figure S3), although $aCDOM_\lambda$ and Φ_λ were usually reported as single values at specific wavelengths in many other studies. In latter cases, full spectra were extrapolated by assuming the same decadic slopes (-0.005 for $aCDOM_\lambda$ and -0.009 for Φ_λ) with wavelength as the available spectra (Figure S3). Note that these slopes are based on log10 of $aCDOM_\lambda$ and Φ_λ, which is the same as exponential slopes -0.012 and -0.021 for commonly reported natural log of $aCDOM_\lambda$ and Φ_λ [9]. We also assumed that, within each type of system, high DOC concentration corresponds to high $aCDOM_\lambda$ and low DOC concentration corresponds to low $aCDOM_\lambda$, due to the fact that DOC concentration and $aCDOM_\lambda$ were usually not reported together.

In streams and rivers, water surface slope (S) and water column depth (H) are expected to co-vary, and both are a function of flow discharge (Q), although from the literature S, H, and Q were usually not reported together. In order to predict S and H from reported values while capturing their covariation, we plotted S-Q and H-Q relationships based on data when S-Q or H-Q were reported together (Figure S4). For streams and rivers, both S and H exhibit power law relationships with discharge, $\log_{10} H = 0.25\log_{10} Q - 0.46$ and $\log_{10} S = -0.12\log_{10} Q - 2.55$. For streams and rivers, S and H can therefore be predicted by the power laws and corresponding prediction intervals, when at least one of *S*, *H*, or *Q* were reported. In beaded streams, existing *S*-*Q* data do not show a clear relationship (Figure S4), and pool structure is expected to behave differently than common streams, so we assumed that ranges of *H* and *S* for beaded streams do not co-vary with *Q*.

SI-3. Non-dimensionalization of the dispersion-reaction equation.

The original dispersion-reaction equation is

$$\frac{\partial C(y,t)}{\partial t} = \frac{\partial}{\partial y}\left(D(y)\frac{\partial C(y,t)}{\partial y}\right) - \sum_{\lambda}\phi_{\lambda} aCDOM_{\lambda}(y,t) Q_{dso-\lambda} e^{-K_{d\lambda}(y)y} \quad \text{(S5)}$$

with non-flux boundary conditions

$$\left.\frac{\partial C(y,t)}{\partial y}\right|_{y=0} = 0 \quad \text{(S6a)}$$

$$\left.\frac{\partial C(y,t)}{\partial y}\right|_{y=H} = 0 \quad \text{(S6b)}$$

where $C(y,t)$ is DOC concentration, *t* is time, *y* is the vertical position that is 0 at water surface and positive in the downward direction, and $D(y)$ is the *y*-dependent vertical dispersion coefficient that dictates vertical mixing and sets the rate of resupply of CDOM from bottom waters to the surface, Φ_{λ} is the photo-lability of CDOM, $Q_{dso-\lambda}$ is the photon flux at the water surface, $aCDOM_{\lambda}(y,t)$ is the light attenuation coefficient of CDOM, and $K_{d\lambda}(y)$ is the total light attenuation coefficient. Notations in this study are summarized in Table S3.

The dimensional variables contained in (S5) are *C*, *t*, and *y*. Thus, the dimensions to be normalized are concentration, time, and length. We define the following scales to normalize dimensional variables into dimensionless ones.

$$y = Hy^{*} \quad \text{(S7a)}$$

$$C(y,t) = \frac{1}{\varepsilon_{280}H} C^{*}\left(y^{*},t^{*}\right) \quad \text{(S7b)}$$

$$t = \frac{H^{2}}{\langle D(y)\rangle} t^{*} \quad \text{(S7c)}$$

where superscript * indicates dimensionless quantities, ε_{280} denotes empirical parameter ε_{λ} at wavelength 280 nm, and $\langle D\rangle$ is the depth-averaged vertical dispersion coefficient. Wavelength 280 nm was picked because it is the high end of the spectra such that ε_{280} is always non-zero. Plug (S7) into (S5)-(S6), (S5)-(S6) become

$$\begin{aligned}\frac{\partial C^{*}\left(y^{*},t^{*}\right)}{\partial t^{*}} &= \frac{\partial}{\partial y^{*}}\left(\frac{D\left(y^{*}\right)}{\langle D\rangle}\frac{\partial C^{*}\left(y^{*},t^{*}\right)}{\partial y^{*}}\right) \\ &\quad - \frac{H^{2}}{\langle D\rangle}\sum_{\lambda}\phi_{\lambda}\frac{aCDOM_{\lambda}\left(y^{*},t^{*}\right)}{C\left(y^{*},t^{*}\right)} Q_{dso-\lambda} e^{-K_{d\lambda}\left(y^{*}\right)Hy^{*}} C^{*}\left(y^{*},t^{*}\right)\end{aligned} \quad \text{(S8)}$$

with non-flux boundary conditions

$$\left.\frac{\partial C^*\left(y^*,t^*\right)}{\partial y^*}\right|_{y^*=0}=0 \tag{S9a}$$

$$\left.\frac{\partial C^*\left(y^*,t^*\right)}{\partial y^*}\right|_{y^*=1}=0 \tag{S9b}$$

(S8) can be rewritten as

$$\frac{\partial C^*\left(y^*,t^*\right)}{\partial t^*}=\frac{\partial}{\partial y^*}\left(\frac{D\left(y^*\right)}{\langle D\rangle}\frac{\partial C^*\left(y^*,t^*\right)}{\partial y^*}\right)-\sum_{\lambda} d_{\lambda}^* e^{-p_{\lambda}^* y^*} C^*\left(y^*,t^*\right) \tag{S10}$$

where d_{λ}^* and p_{λ}^* are wavelength-specific dimensionless parameters defined by

$$d_{\lambda}^*=\frac{H^2}{\langle D\rangle}\phi_{\lambda}\frac{aCDOM_{\lambda}\left(y^*,t^*\right)}{C\left(y^*,t^*\right)}Q_{dso-\lambda} \tag{S11a}$$

$$p_{\lambda}^*=K_{d\lambda}\left(y^*\right)H \tag{S11b}$$

SI-4. Solving for the depth-integrated photomineralization rate.

The generalized dispersion-reaction equation is:

$$\frac{\partial C^*\left(y^*,t^*\right)}{\partial t^*}=\frac{\partial}{\partial y^*}\left(\frac{D\left(y^*\right)}{\langle D\rangle}\frac{\partial C^*\left(y^*,t^*\right)}{\partial y^*}\right)-d^* e^{-p^* y^*} C^*\left(y^*,t^*\right) \tag{S12}$$

with non-flux boundary condition (S9), where d^* is surface Damkohler number, and p^* is dimensionless light attenuation. The moment method[10] solves for the dimensionless depth-integrated photomineralization rate, r^*, as well as the vertical distribution of DOC concentration, at asymptotic regime. At the asymptotic regime, the dimensionless depth-averaged DOC concentration decays at a first-order rate constant r^* over time[10]

$$\frac{d<C^*>}{dt^*}=r^*<C^*> \tag{S13}$$

The moment method defines a representative unit cell, where the vertical water column is mirrored, such that reaction and dispersion profiles are symmetric about $y^*=0$. The governing equation within a unit cell becomes:

$$\frac{\partial C^*\left(y^*,t^*\right)}{\partial t^*}=\frac{\partial}{\partial y^*}\left(D^*\left(\left|y^*\right|\right)\frac{\partial C^*\left(y^*,t^*\right)}{\partial y^*}\right)-d^* e^{-p^*\left|y^*\right|} C^*\left(y^*,t^*\right) \tag{S14}$$

with periodic boundary conditions:

$$C^*\left(y^*=-1,t^*\right)=C^*\left(y^*=1,t^*\right) \tag{S15a}$$

$$\left.\frac{\partial C^*\left(y^*,t^*\right)}{\partial y^*}\right|_{y^*=-1}=\left.\frac{\partial C^*\left(y^*,t^*\right)}{\partial y^*}\right|_{y^*=1} \tag{S15b}$$

At asymptotic regime, DOC concentration has been fully developed in the unit cell, such that solute concentration is symmetric about $y^*=0$. Therefore, non-flux boundary condition (S9) applies in vertical water column.

The asymptotic regime solution r^* is given by the smallest eigenvalue of the following eigenvalue problem[10, 11]

$$\frac{d}{dy^*}\left(D^*\left(\left|y^*\right|\right)\frac{dE\left(y^*\right)}{dy^*}\right)-d^*e^{-p^*\left|y^*\right|}E\left(y^*\right)=-\Lambda E\left(y^*\right) \tag{S16}$$

with periodic boundary conditions:

$$E\left(y^*=-1\right)=E\left(y^*=1\right) \tag{S17a}$$

$$\left.\frac{dE\left(y^*\right)}{dy^*}\right|_{y^*=-1}=\left.\frac{dE\left(y^*\right)}{dy^*}\right|_{y^*=1} \tag{S17b}$$

where $E(y^*)$ is the eigenfunction and Λ is the eigenvector. The eigenvector that corresponds to the smallest eigenvalue is the vertical distribution of DOC concentration at asymptotic regime.

We used finite difference method to solve the eigenvalue problem (S16)-(S17). We discretized the vertical water column into $n+1$ layers ($n = 1024$). The unit cell is therefore discretized into $2n+2$ layers, each with thickness $h = \frac{1}{n+1}$. For each layer i ($i = 0, 1, \ldots, 2n+1$) within the unit cell, denote $y_i^* \equiv -1 + hi$ such that $y_0^* = -1$ and $y_{n+1}^* = 0$. Denote $D_i^* \equiv D^*\left(y_i^*\right)$ and $E_i \equiv E\left(y_i^*\right)$, (S12) becomes

$$\frac{D^*_{i+\frac{1}{2}}E_{i+1}}{h^2}+\frac{D^*_{i-\frac{1}{2}}E_{i-1}}{h^2}-\frac{(D^*_{i+\frac{1}{2}}+D^*_{i-\frac{1}{2}})E_i}{h^2}-d^*e^{-p^*y_i^*}E_i=-\Lambda E_i \tag{S18}$$

Define

$$\eta_i \equiv -\frac{(D^*_{i+\frac{1}{2}}+D^*_{i-\frac{1}{2}})}{h^2}-d^*e^{-p^*y_i^*} \tag{S19a}$$

$$\theta_i \equiv \frac{D^*_{i+\frac{1}{2}}}{h^2} \tag{S19b}$$

$$\xi_i \equiv \frac{D^*_{i-\frac{1}{2}}}{h^2} \tag{S19c}$$

(S18) becomes

$$\xi_i E_{i-1}+\eta_i E_i+\theta_i E_{i+1}=-\Lambda E_i \tag{S20}$$

With periodic boundary conditions (S17) applied, (S20) can be written as

$$-\begin{pmatrix} \eta_0 & \theta_0 & 0 & \cdots & 0 & 0 & \xi_0 \\ \xi_1 & \eta_1 & \theta_1 & \cdots & 0 & 0 & 0 \\ 0 & \xi_2 & \eta_2 & \cdots & 0 & 0 & 0 \\ & & & \ddots & & & \\ 0 & 0 & 0 & \cdots & \eta_{2n-1} & \theta_{2n-1} & 0 \\ 0 & 0 & 0 & \cdots & \xi_{2n} & \eta_{2n} & \theta_{n-1} \\ \theta_{2n+1} & 0 & 0 & \cdots & 0 & \xi_{2n+1} & \eta_{2n+1} \end{pmatrix} \begin{pmatrix} E_0 \\ E_1 \\ E_2 \\ \vdots \\ E_{2n-1} \\ E_{2n} \\ E_{2n+1} \end{pmatrix} = \Lambda \begin{pmatrix} E_0 \\ E_1 \\ E_2 \\ \vdots \\ E_{2n-1} \\ E_{2n} \\ E_{2n+1} \end{pmatrix} \tag{S21}$$

To this point, the smallest eigenvalue and the corresponding eigenvector can be solved.

SI-5. Estimating vertical dispersion profiles of arctic waters.

In the Kuparuk River, the vertical dispersion coefficient $D(y)$ follows a standard model[12, 13]:

$$D(y) = \kappa u_* y\left(1 - \frac{y}{H}\right) \tag{S22}$$

where κ is the von Karman constant, u_* is the shear velocity [m s^{-1}], and H is the water column depth [m]. Because the observed river channel width is always at least 10 times larger than the observed river depth, turbulent properties are independent of river width[12]. Therefore, we approximate the shear velocity by $u_* = \sqrt{gHS}$, where g is gravitational acceleration [m s^{-2}] and S is the water surface slope. The depth-averaged vertical dispersion coefficient therefore is

$$\left\langle D\left(y^*\right)\right\rangle = \frac{\kappa}{6} u_* H \tag{S23}$$

We assume arctic streams and rivers to follow the same vertical dispersion profile as equation (S22). Arctic lakes and beaded stream pools usually have more complicated dispersion profiles. We assume two scenarios to capture the natural ranges of vertical mixing in beaded stream pools: the vertical dispersion profile in equation (S22) at fast flow, and a layered dispersion profile at slow flow. In the latter case, we assume that the top 10% of the pool depth mixes rapidly at the mean dispersion value of the fast flow scenario, while the deep layer of the pool mixes 2 orders of magnitude slower, a typical ratio for lakes worldwide[14-16].

$$D(y) = \begin{cases} \dfrac{\kappa}{6} u_* H, & y \le 10\% H \\ 1\% \dfrac{\kappa}{6} u_* H, & y > 10\% H \end{cases} \tag{S24}$$

In arctic lakes, because the epilimnion (or the surface layer) usually defines a turbulent mixing layer that has much higher vertical dispersion than the deep layer, we define two scenarios of vertical dispersion: deep lakes that are deeper than the mean epilimnion depth in arctic lakes, and shallow lakes that are shallower than the mean epilimnion depth. Water transparency and mixing depth often relates to each other, because rapid absorption of light at the surface often creates a "trapping depth" defined by a high density gradient[17]. A strong relationship between transparency and mixing depth was found in a variety of lakes, including those larger than Toolik Lake (1.5 km^2 fetch) and those that are sheltered from the wind (crater lakes)[18]. Even in sheltered lakes where diurnal thermoclines are more common during solar heating and calm conditions, the longer-term, average mixing depth is still related strongly to the optical properties of the water[18-20]. Secchi depth, which characterizes the optical property of the water column, strongly affects epilimnion depth in relatively small temperate lakes (defined as fetch < 500 ha in [20]), and becomes less effective in predicting epilimnion depth of large temperate lakes (defined as fetch > 500 ha in [20]). However, very large lakes in the Arctic are rare compared to temperate lakes, and studies typically report a much smaller range of fetch (0.003-1.5 km2, which is 0.3-150 ha, based on 7 studies of 51 arctic lake)[21-27]. Further, given that arctic waters are typically light limited and have high CDOM, even if mixing is confined to a near-surface layer, the amount CDOM is difficult to consume in short periods of time (days to weeks), and CDOM would be resupplied from greater depths as soon as a diurnal thermocline is erased, for example by wind mixing or convective mixing at night[28]. Therefore, Secchi depth was chosen to estimate epilimnion depth. We estimate the mean epilimnion depth in arctic lakes using an empirical relationship with Secchi depth reported for temperate-zone lakes[19], assuming that arctic lakes behave similarly to temperate-zone lakes

$$\overline{E}_d = 3.24 + 0.35\overline{S}_d \tag{S25}$$

where $\overline{E}_d$ is the mean epilimnion depth (4.3 m) and $\overline{S}_d$ is the mean Secchi depth reported in arctic lakes. In shallow lakes, we treat the entire water column as the surface layer where vertical dispersion is uniform over depth and spans the range 10^{-5}–10^{-2} $m^2\,s^{-1}$. In deep lakes, we assumed that deep-layer dispersion is 2 orders of magnitude lower than surface layer dispersion, which is representative of reported ranges for lakes and oceans[14-16]. For each deep lake, given that Secchi depth and lake depth are usually not reported together (Table S1), we assumed that the epilimnion depth (or the surface layer thickness) E_d can be estimated by

$$E_d = \frac{\overline{E}_d}{\overline{H}_{DL}} H \tag{S26}$$

where $\overline{H}_{DL}$ is the mean depth of deep arctic lakes (12.5 m). (S26) only serves as a rough estimate of E_d for each deep lake system.

Table S1. Data sources of photochemical and hydrological parameters in arctic stream, rivers, beaded streams, and lakes.

	DOC	$aCDOM_{\lambda}$	Φ_{λ}	*Q*	*H*	*S*	*SD*
rivers	1, 7, 29-32	1, 7, 32	1, 7	2, 32-35	2, 35	2, 33, 34	-
streams	1, 7, 29-31, 36, 37	1, 7, 38	1, 7	2, 33, 35, 36, 39, 40	2, 35	2, 33, 34, 39, 40	-
beaded streams	1, 29-31, 41-44	38, 41, 43	1, 41, 42	33, 38-40, 43-47	38, 44-47	33, 39, 40, 45, 47	-
lakes	7, 21, 26, 31, 37, 48-52	1, 7	1, 7	-	21-27, 48, 49, 53	-	31, 54-58

* From left to right, *DOC*, $aCDOM_{\lambda}$, Φ_{λ}, *Q*, *H*, *S*, and *SD* denote DOC concentration, light attenuation coefficient of CDOM, photo-lability of CDOM, flow discharge, water column depth, water surface slope, and Secchi depth respectively. The reference numbers correspond to the references in SI.

Table S2. Reported ranges (min, max) of photochemical and hydrological parameters in arctic streams and rivers (rocky bottom), beaded streams (peat bottom), and lakes.

	DOC (mol m^{-3})	$aCDOM_{300}$ (m^{-1})	Φ_{300} (mol CO_2 mol^{-1} photon)	*H* (m)	*S* (-)	*SD* (m)
rivers	0.028, 18	3.6, 103	4×10^{-4}, 0.08	0.14, 15.5	5×10^{-5}, 0.03	-
streams	0.028, 18	4.6, 334	5×10^{-4}, 0.04	0.015, 2.1	1.7×10^{-4}, 0.1	-
beaded streams	0.12, 3.1	33, 359	0.003, 0.04	0.12, 3.0	3×10^{-4}, 0.009	-
lakes	0.008, 2.7	4.3, 79	4×10^{-4}, 0.08	0.08, 43	-	0.3, 11.2

* Nomenclatures same as Table S1. Light attenuation coefficient of CDOM ($aCDOM_{\lambda}$) and photo-lability of CDOM (Φ_{λ}) are adjusted to wavelength = 300 nm.

Table S3. (A) Percentage of systems partially or substantially limited by mixing for each type of arctic systems that exhibit exponential light attenuation over depth. (B) Depth-integrated attenuation ratio (mean ± standard error) for each type of arctic systems that are partially or substantially limited by mixing.

(A) Percentage within each type of arctic systems

	partially limited	substantially limited
streams and rivers	0%	0%
beaded streams	0.1%	0%
lakes	12%	30%

(B) Depth-integrated attenuation ratio

	partially limited	substantially limited
streams and rivers	---	---
beaded streams	0.92±0.001	---
lakes	0.95±0.001	0.58±0.002

Table S4. List of notations.

English letters

$aCDOM_{\lambda}$ [m^{-1}]	light attenuation coefficient of CDOM
aSS_{λ} [m^{-1}]	light attenuation coefficient of suspended sediment (SS)
C [mol m^{-3}]	DOC concentration
D [m^2 s^{-1}]	vertical dispersion coefficient
d^*	surface Damkohler number
E	eigenfunction
E_d [m]	epilimnion depth
g [m s^{-2}]	gravitational acceleration
H [m]	water column depth
$\bar{H}_{DL}$ [m]	mean depth of deep arctic lakes
$K_{d\lambda}$ [m^{-1}]	total light attenuation coefficient
p^*	dimensionless light attenuation
P_e	statistical equilibrium of the vertical distribution of DOC
PM [mol m^{-3} s^{-1}]	DOC photo-mineralization rate
Q [m^{-3} s^{-1}]	discharge
$Q_{dso-\lambda}$ [mol m^{-2} s^{-1}]	photon flux at the water surface
Q_{λ} [mol m^{-2} s^{-1}]	photon flux
r [s^{-1}]	depth-integrated photomineralization rate
r_{wm} [s^{-1}]	depth-integrated photomineralization rate under well-mixed assumption
S	water surface slope
S_d [m]	Secchi depth
t [s]	time
u_* [m s^{-1}]	shear velocity
W [m]	river width
y [m]	vertical position in the water column

Greek letters

α_{λ} [m^{-1}]	$aCDOM_{\lambda} = \begin{cases} \alpha_{\lambda} + \varepsilon_{\lambda} C & if \quad \alpha_{\lambda} + \varepsilon_{\lambda} C > 0 \\ 0 & if \quad \alpha_{\lambda} + \varepsilon_{\lambda} C \le 0 \end{cases}$
ε_{λ} [m^2 mol^{-1}]	
η_{react}	reaction efficiency
κ	von Karman constant
Λ	eigenvector
λ [m]	wavelength
ϕ_{λ} [mol CO_2 mol^{-1} photon]	photo-lability of CDOM to photomineralization, also known as the apparent quantum yield for photomineralization

Others

superscript *	dimensionless variable or parameter

$\langle\rangle$	depth-averaged value
$\bar{}$	mean value

References

1. R. M. Cory, C. P. Ward, B. C. Crump and G. W. Kling, Sunlight controls water column processing of carbon in arctic fresh waters, *Science*, 2014, **345**, 925-928.
2. T. V. King, B. T. Neilson, L. D. Overbeck and D. L. Kane, Water temperature controls in low arctic rivers, *Water Resources Research*, 2016, **52**, 4358-4376.
3. G. W. Kling and R. M. Cory, Biogeochemistry data set for NSF Arctic Photochemistry project on the North Slope of Alaska, *Environmental Data Initiative*, 2015, http://dx.doi.org/10.6073/pasta/22a3a3fc2dc74b7aabe8a10ab9061cf0.
4. G. W. Kling and R. M. Cory, Photochemistry data set for NSF Photochemistry project on the North Slope of Alaska, 2015, http://dx.doi.org/10.6073/pasta/2f9433d6a608e82e1dd4fa23175c1f59.
5. G. W. Kling and R. M. Cory, Light profile data set for NSF Photochemistry project on the North Slope of Alaska, *Environmental Data Initiative*, 2015, http://dx.doi.org/10.6073/pasta/8e8cb22fd7ee278168f8eb6ad7e1a48c.
6. G. W. C. Kling, R. M., Apparent quantum yield data set for NSF Photochemistry project on the North Slope of Alaska, *Environmental Data Initiative*, 2015, http://dx.doi.org/10.6073/pasta/aa2d0ed4ddef6e76c3ef8d6c12460607.
7. R. M. Cory, B. C. Crump, J. A. Dobkowski and G. W. Kling, Surface exposure to sunlight stimulates CO2 release from permafrost soil carbon in the Arctic, *Proceedings of the National Academy of Sciences of the United States of America*, 2013, **110**, 3429-3434.
8. J. D. J. Ingle and S. R. Crouch, Spectrochemical analysis, 1988.
9. C. L. Osburn, N. J. Anderson, C. A. Stedmon, M. E. Giles, E. J. Whiteford, T. J. McGenity, A. J. Dumbrell and G. J. Underwood, Shifts in the Source and Composition of Dissolved Organic Matter in Southwest Greenland Lakes Along a Regional Hydro-climatic Gradient, *Journal of Geophysical Research: Biogeosciences*, 2017, **122**, 3431-3445.
10. M. Shapiro and H. Brenner, Dispersion of a chemically reactive solute in a spatially periodic model of a porous medium, *Chemical Engineering Science*, 1988, **43**, 551-571.
11. B. B. Dykaar and P. K. Kitanidis, Macrotransport of a biologically reacting solute through porous media, *Water Resources Research*, 1996, **32**, 307-320.
12. H. B. Fischer, J. E. List, C. R. Koh, J. Imberger and N. H. Brooks, *Mixing in inland and coastal waters*, Academic Press, San Diego, CA, 1979.
13. M. R. Leeder, *Sedimentology and sedimentary basins: from turbulence to tectonics*, Wiley-Blackwell, Oxford, U.K., 2nd edn., 2011.
14. S. W. Zison, *Rates, constants, and kinetics formulations in surface water quality modeling*, Environmental Protection Agency, Environmental Research Laboratory, Athens, GA, 1978.
15. G. E. Likens, *Biogeochemistry of inland waters*, Academic Press, San Diego, CA, 2010.
16. S. C. Chapra, *Surface water-quality modeling*, Waveland press, Long Grove, IL, 2008.
17. J. F. Price, R. A. Weller and R. Pinkel, Diurnal cycling: Observations and models of the upper ocean response to diurnal heating, cooling, and wind mixing, *Journal of Geophysical Research: Oceans*, 1986, **91**, 8411-8427.
18. G. W. Kling, Comparative transparency, depth of mixing, and stability of stratification in lakes of Cameroon, West Africa1, *Limnology Oceanography*, 1988, **33**, 27-40.

19. A. Mazumder and W. D. Taylor, Thermal structure of lakes varying in size and water clarity, *Limnology and Oceanography*, 1994, **39**, 968-976.
20. E. Fee, R. Hecky, S. Kasian and D. Cruikshank, Effects of lake size, water clarity, and climatic variability on mixing depths in Canadian Shield lakes, *Limnology Oceanography*, 1996, **41**, 912-920.
21. J. E. Hobbie and G. W. Kling, *Alaska's changing Arctic: Ecological consequences for tundra, streams, and lakes*, Oxford University Press, 2014.
22. M. H. Hermanson, Anthropogenic mercury deposition to Arctic lake sediments, *Water, Air, and Soil Pollution*, 1998, **101**, 309-321.
23. P. T. Doran, C. P. McKay, W. P. Adams, M. C. English, R. A. Wharton and M. A. Meyer, Climate forcing and thermal feedback of residual lake-ice covers in the high Arctic, *Limnology and Oceanography*, 1996, **41**, 839-848.
24. A. Evenset, G. N. Christensen, T. Skotvold, E. Fjeld, M. Schlabach, E. Wartena and D. Gregor, A comparison of organic contaminants in two high Arctic lake ecosystems, Bjørnøya (Bear Island), Norway, *Science of the Total Environment*, 2004, **318**, 125-141.
25. B. M. Jones, C. D. Arp, K. M. Hinkel, R. A. Beck, J. A. Schmutz and B. Winston, Arctic lake physical processes and regimes with implications for winter water availability and management in the National Petroleum Reserve Alaska, *Environmental Management*, 2009, **43**, 1071-1084.
26. S. Kokelj, R. Jenkins, D. Milburn, C. Burn and N. Snow, The influence of thermokarst disturbance on the water quality of small upland lakes, Mackenzie Delta region, Northwest Territories, Canada, *Permafrost and Periglacial Processes*, 2005, **16**, 343-353.
27. D. Schindler, J. Kalff, H. Welch, G. Brunskill, H. Kling and N. Kritsch, Eutrophication in the high arctic-meretta lake, cornwallis island (75 N lat.), *Journal of the Fisheries Board of Canada*, 1974, **31**, 647-662.
28. S. MacIntyre, J. P. Fram, P. J. Kushner, N. D. Bettez, W. O'brien, J. Hobbie and G. W. Kling, Climate-related variations in mixing dynamics in an Alaskan arctic lake, *Limnology Oceanography*, 2009, **54**, 2401-2417.
29. W. B. Bowden, ArcLTER streams chemistry data 1983 to present, *Environmental Data Initiative*, 2016, http://dx.doi.org/10.6073/pasta/8b81b5b0cf936c8b2bb173adab506fd7.
30. J. R. Larouche, B. W. Abbott, W. B. Bowden and J. B. Jones, The role of watershed characteristics, permafrost thaw, and wildfire on dissolved organic carbon biodegradability and water chemistry in Arctic headwater streams, *Biogeosciences*, 2015, **12**, 4221-4233.
31. G. W. Kling, Chemistry from thermokarst impacted soils, lakes, and streams near Toolik Lake Alaska, 2008-2011, *Environmental Data Initiative*, 2012, http://dx.doi.org/10.6073/pasta/2e55d1587290e642938ac1a6caed6ec6.
32. P. Mann, R. Spencer, P. Hernes, J. Six, G. Aiken, S. Tank, J. McClelland, K. Butler, R. Dyda and R. Holmes, Pan-arctic trends in terrestrial dissolved organic matter from optical measurements, *Earth Sci*, 2016, **4**, 25.
33. K. J. Edwardson, W. B. Bowden, C. Dahm and J. Morrice, The hydraulic characteristics and geochemistry of hyporheic and parafluvial zones in Arctic tundra streams, north slope, Alaska, *Advances in Water Resources*, 2003, **26**, 907-923.
34. K. M. Scott, *Effects of permafrost on stream channel behavior in Arctic Alaska*, US Govt. Print. Off., 1978.

35. W. M. Wollheim, B. J. Peterson, L. A. Deegan, J. E. Hobbie, B. Hooker, W. B. Bowden, K. J. Edwardson, D. B. Arscott, A. E. Hershey and J. Finlay, Influence of stream size on ammonium and suspended particulate nitrogen processing, *Limnology and Oceanography*, 2001, **46**, 1-13.
36. B. C. Crump, G. W. Kling, M. Bahr and J. E. Hobbie, Bacterioplankton community shifts in an arctic lake correlate with seasonal changes in organic matter source, *Applied and Environmental Microbiology*, 2003, **69**, 2253-2268.
37. G. W. Kling, G. W. Kipphut, M. M. Miller and W. J. O'Brien, Integration of lakes and streams in a landscape perspective: the importance of material processing on spatial patterns and temporal coherence, *Freshwater Biology*, 2000, **43**, 477-497.
38. M. Merck, B. Neilson, R. Cory and G. Kling, Variability of in-stream and riparian storage in a beaded arctic stream, *Hydrological Processes*, 2012, **26**, 2938-2950.
39. M. J. Greenwald, W. B. Bowden, M. N. Gooseff, J. P. Zarnetske, J. P. McNamara, J. H. Bradford and T. R. Brosten, Hyporheic exchange and water chemistry of two arctic tundra streams of contrasting geomorphology, *Journal of Geophysical Research: Biogeosciences*, 2008, **113**.
40. J. P. Zarnetske, M. N. Gooseff, T. R. Brosten, J. H. Bradford, J. P. McNamara and W. B. Bowden, Transient storage as a function of geomorphology, discharge, and permafrost active layer conditions in Arctic tundra streams, *Water Resources Research*, 2007, **43**.
41. R. M. Cory, K. H. Harrold, B. T. Neilson and G. W. Kling, Controls on dissolved organic matter (DOM) degradation in a headwater stream: the influence of photochemical and hydrological conditions in determining light-limitation or substrate-limitation of photo-degradation, *Biogeosciences*, 2015, **12**, 6669-6685.
42. G. W. Kling, Biogeochemistry data set for Imnavait Creek Weir on the North Slope of Alaska, *Environmental Data Initiative*, 2015, http://dx.doi.org/10.6073/pasta/f540d09369a9065704df7df669270836.
43. B. L. Miller, Terrestrial-aquatic transfers of carbon dioxide, methane, and organic carbon from riparian wetlands to an arctic headwater stream, M.S., University of Michigan at Ann Arbor, 2014.
44. M. Oswood, J. Irons III and D. Schell, in *Landscape function and disturbance in arctic tundra*, Springer, 1996, pp. 275-289.
45. C. D. Arp, M. S. Whitman, B. M. Jones, G. Grosse, B. V. Gaglioti and K. C. Heim, Distribution and biophysical processes of beaded streams in Arctic permafrost landscapes, *Biogeosciences*, 2015, **12**, 29-47.
46. M. Oswood, K. Everett and D. Schell, Some physical and chemical characteristics of an arctic beaded stream, *Holarctic Ecology*, 1989, **12**, 290-295.
47. A. Tarbeeva and V. Surkov, Beaded channels of small rivers in permafrost zones, *Geography and Natural Resources*, 2013, **34**, 216-220.
48. M. Amyot, D. Lean and G. Mierle, Photochemical formation of volatile mercury in high Arctic lakes, *Environmental Toxicology and Chemistry*, 1997, **16**, 2054-2063.
49. P. B. Hamilton, K. Gajewski, D. E. Atkinson and D. R. Lean, Physical and chemical limnology of 204 lakes from the Canadian Arctic Archipelago, *Hydrobiologia*, 2001, **457**, 133-148.
50. D. P. Morris, H. Zagarese, C. E. Williamson, E. G. Balseiro, B. R. Hargreaves, B. Modenutti, R. Moeller and C. Queimalinos, The attenuation of solar UV radiation in

lakes and the role of dissolved organic carbon, *Limnology and Oceanography*, 1995, **40**, 1381-1391.
51. S. Sobek, L. J. Tranvik, Y. T. Prairie, P. Kortelainen and J. J. Cole, Patterns and regulation of dissolved organic carbon: An analysis of 7,500 widely distributed lakes, *Limnology and Oceanography*, 2007, **52**, 1208-1219.
52. S. E. Tank, L. F. Lesack, J. A. Gareis, C. L. Osburn and R. H. Hesslein, Multiple tracers demonstrate distinct sources of dissolved organic matter to lakes of the Mackenzie Delta, western Canadian Arctic, 2011.
53. G. W. Kling, G. W. Kipphut and M. C. Miller, The flux of CO2 and CH4 from lakes and rivers in arctic Alaska, *Hydrobiologia*, 1992, **240**, 23-36.
54. A. K. Giblin, George W, Physical and chemical data for various lakes near Toolik Research Station, Arctic LTER. Summer 1983 to 1989, *Environmental Data Initiative*, 2015, http://dx.doi.org/10.6073/pasta/1f780cc1b9e31f58a87d72b8eb2693ea.
55. A. K. Giblin, George W, Physical and chemical data for various lakes near Toolik Research Station, Arctic LTER. Summer 1990 to 1999, *Environmental Data Initiative*, 2015, http://dx.doi.org/10.6073/pasta/1fd85582de93a281e5e5d3b80df97b52.
56. A. K. Giblin, George W, Physical and chemical data for various lakes near Toolik Research Station, Arctic LTER. Summer 2000 to 2009, *Environmental Data Initiative*, 2015, http://dx.doi.org/10.6073/pasta/791e3cb6288f75f602f23ef3e5532017.
57. A. K. Giblin, George W, Physical and chemical data for various lakes near Toolik Research Station, Arctic LTER. Summer 2010 to 2014, *Environmental Data Initiative*, 2015, http://dx.doi.org/10.6073/pasta/2d161db112e1855277c112d9b4ffc980.
58. G. W. Kling, Biogeochemistry data set for soil waters, streams, and lakes near Toolik on the North Slope of Alaska, *Environmental Data Initiative*, 2016, http://dx.doi.org/10.6073/pasta/e240e6b082d5536e1c9dd2d2ddc2e88b.